Supplement of Earth Surf. Dynam., 12, 201–218, 2024
https://doi.org/10.5194/esurf-12-201-2024-supplement

Earth Surface Dynamics
Open Access
EGU

Supplement of

Statistical characterization of erosion and sediment transport mechanics in shallow tidal environments – Part 2: Suspended sediment dynamics

Davide Tognin et al.

Correspondence to: Davide Tognin (davide.tognin@unipd.it)

Supplement

1 The Sediment Transport and Bed Evolution Module

1.1 The stochastic approach for the computation of the transport parameter

The transport parameter, T, is usually defined as

$$T = \max\left\{0; \frac{\tau_{wc}}{\tau_c} - 1\right\} \tag{1}$$

where τ_{wc} is the total bottom shear stress and τ_c is the critical shear stress for erosion. This definition describes a sharp transition between $T = 0$ and $T = \tau_{wc}/\tau_c - 1$ that cannot take into account the spatial and temporal variability of both τ_{wc} and τ_c in real tidal systems. Indeed, the bottom shear stress is very unsteady because of the non-uniform flow velocity, wave characteristics and small-scale bottom heterogeneity within a computational element, while the critical shear stress is also affected by the random grain exposure and bed composition in time and space.

Similarly to the stochastic approach proposed by Grass (1970), we assume that both bed shear stress, τ_{wc}, and critical shear stress, τ_c, are random and distributed according to a log-normal probability density function (Grass, 1970; Bridge and Bennett, 1992). Therefore, we can write

$$T = \frac{1}{\tau_c} \int_0^\infty \left[\int_{\tilde{\tau_c}}^\infty (\tilde{\tau_{wc}} - \tilde{\tau_c}) \cdot p_{wc}(\tilde{\tau_{wc}}) d\tilde{\tau_{wc}} \right] \cdot p_c(\tilde{\tau_c}) d\tilde{\tau_c} \tag{2}$$

where $p_{wc}(\bullet)$ and $p_c(\bullet)$ are the probability density function of τ_{wc} and τ_c respectively, and $\tilde{\tau_{wc}}$, $\tilde{\tau_c}$ are the correspondent dummy variables of integration.

The result of this stochastic approach is a smooth transition between $T = 0$ and $T = \tau_{wc}/\tau_c - 1$.

An adequate interpolation of Eq. 2, which is implemented in the numerical model, is given by

$$T = -1 + \left(1 + \left(\frac{\tau_b}{\tau_c}\right)^{\varepsilon}\right)^{1/\varepsilon} \tag{3}$$

where ε is a non-dimensional calibration parameter, that accounts for the shape of the log-normal distribution.

We report here as an example a comparison of the measured and computed SSC at the LT7 station (see Figure S2) for an intense north-easterly Bora wind event in April 2003 (Figure S3). Numerical simulations were performed either by using the classic formulation (Eq. 1) (black thin line) or computing T considering Eq. 3. Using the classic formulation, the model is not able to correctly compute the time evolution of the local turbidity at near-threshold conditions, especially at the beginning of the event (first peak on the 2nd April 2003). On the contrary, the agreement between measured and computed data is quite good when using the stochastic approach.

1.2 Model calibration

The calibration of the model was performed for different periods when SSC field measurements are available (Figure S2, but, for the sake of brevity, we report in the following some examples related to intense and weak resuspension events, referring the reader to Carniello et al. (2012) for a more detailed analysis. Model capability to capture the process is evaluated by means of the Nash-Sutcliffe Model Efficiency (NSE) (Allen et al., 2007).

Focusing on intense resuspension events, we report in the following the results of three periods characterized by intense wind speed, namely: i) 2–5 April 2003 characterized by Bora wind with speeds up to 16 m/s; ii) 9–13 December 2005 characterized by Bora wind with speeds up to 20 m/s; iii) 29 July–2 August 2007 characterized by Bora wind with speeds up to 20 m/s. The comparison with measured data for simulations with an intense wind event in different stations located within the lagoon shows that the model performance to reproduce SSC is from very good to excellent (NSE_{mean} = 0.70, NSE_{median} = 0.67, NSE_{std} = 0.13). In these inner stations, the main contribution to SSC is provided by the mud fraction being negligible the sand content far from the inlets. Interestingly, the model not only correctly predicts the magnitude of the SSC but also captures its modulation induced by tidal level and wind-wave variations (Figure S4).

Additional tests were also carried out considering events characterized by very low wind speed. In particular, we report the results for the period 12-18 April 2006 when turbidity data at six stations close to three inlets are available. At these locations, the sand contribution to the computed SSC is relatively large and of the same order of magnitude as mud contribution (i.e. mud concentration $\sim$10 mg/l and sand concentration $\sim$2–3 mg/l) because close to the inlets the bed composition is richer in sand content than in the inner lagoon. Also in this case the model performance is rated from very good to excellent (NSE_{mean} = 0.62, NSE_{median} = 0.59, NSE_{std} = 0.21). The numerical model correctly reproduces SSC also in the case of very low wind velocity, when the measured SSC can be one order of magnitude lower than that measured with high wind speed (Figure S5).

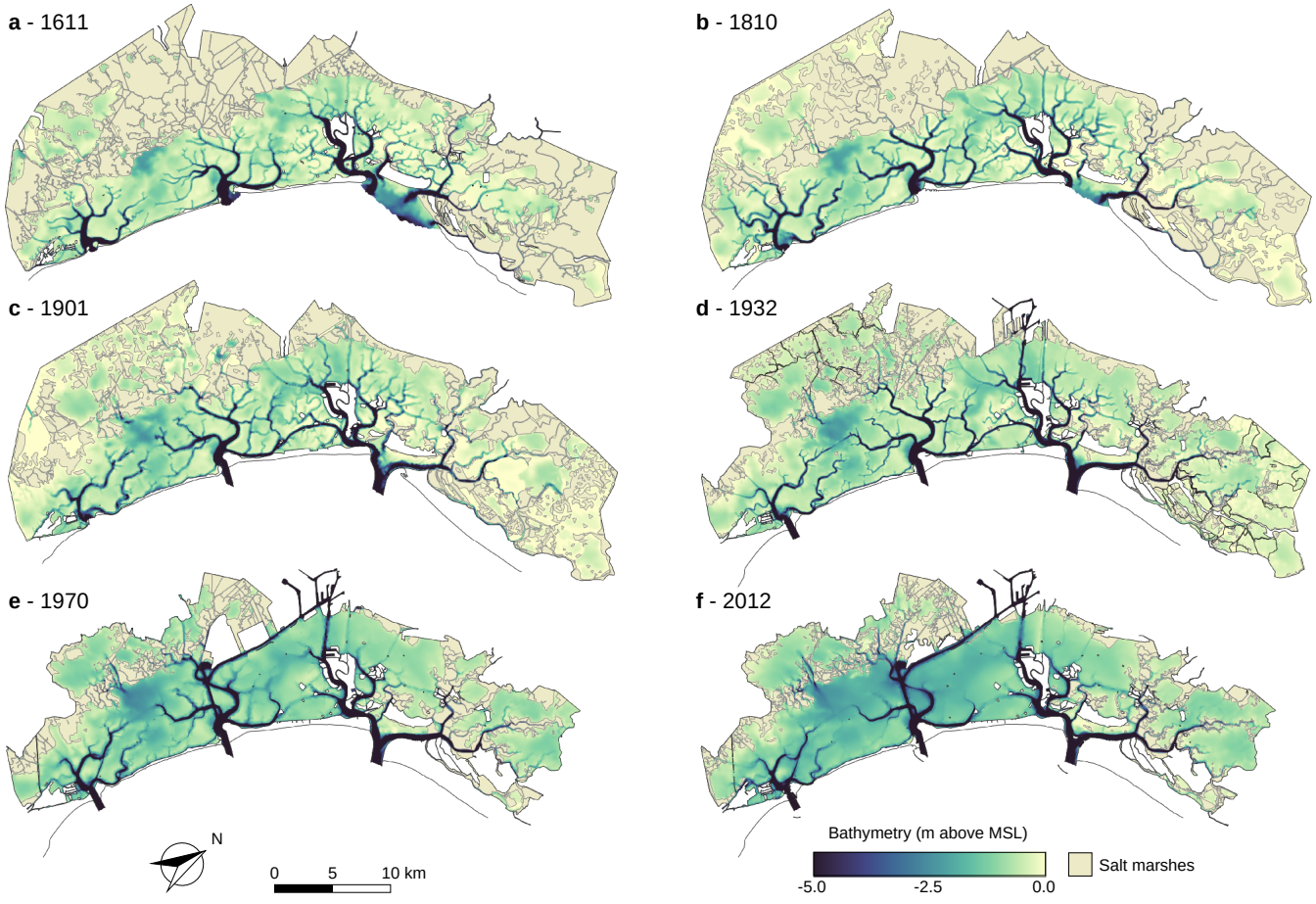

Figure S1. Historical bathymetries of the Venice Lagoon. Color-coded bathymetries of the six different configurations of the Venice Lagoon: (**a**) 1611, (**b**) 1810, (**c**) 1901, (**d**) 1932, (**e**) 1970, and (**f**) 2012.

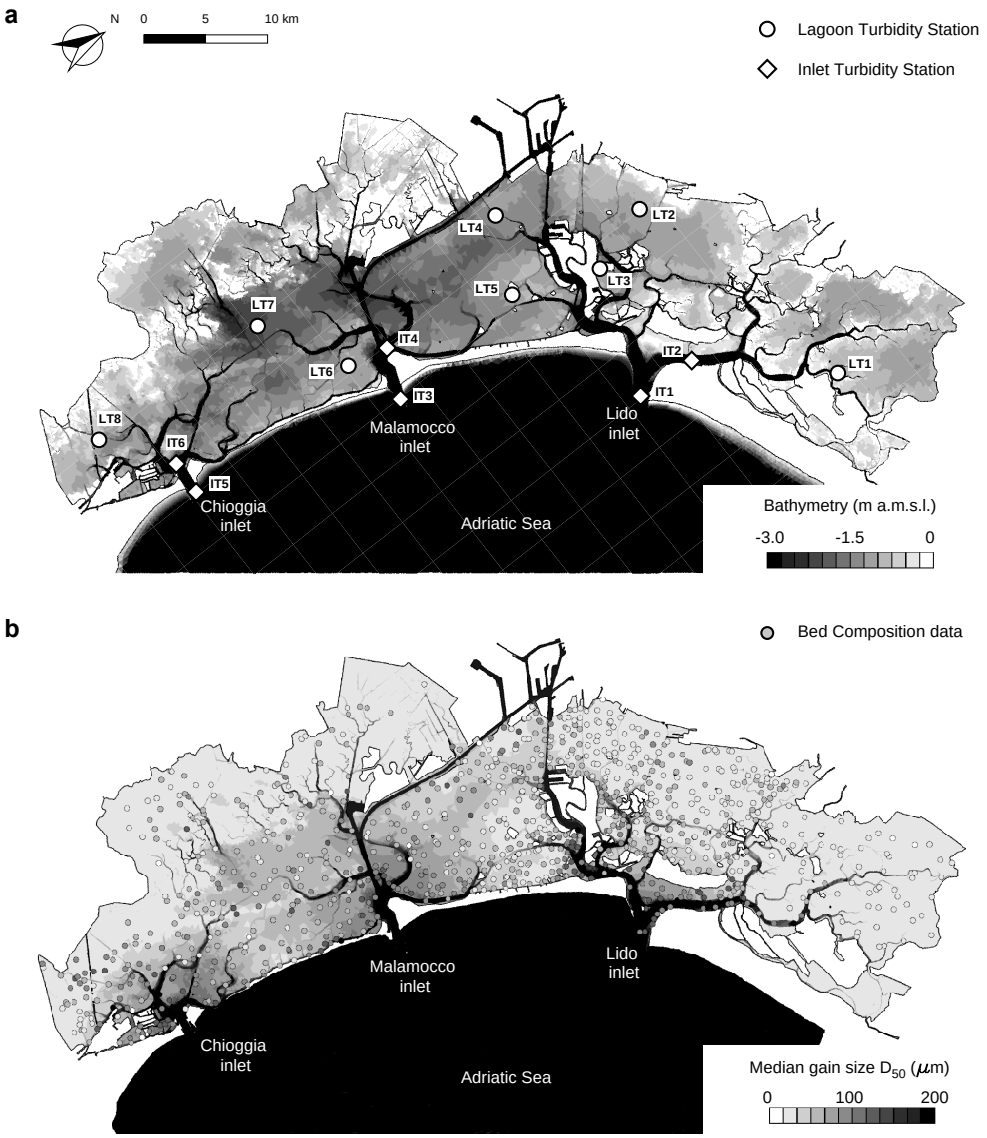

Figure S2. Turbidity and bed sediment grain size data. (**a**) Position of the turbidity stations within the Venice lagoon (LT) and at the inlets (IT). (**b**) Bed composition represented as median grain size D_{50} from measurements (dot) and interpolated (color-coded map).

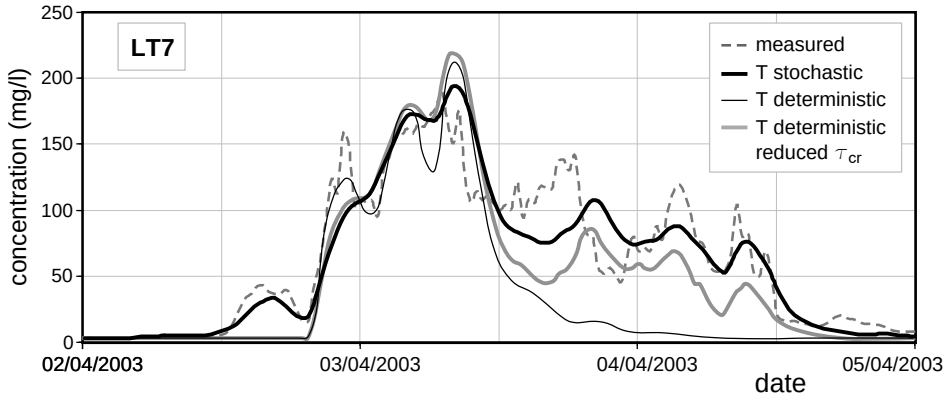

Figure S3. Stochastic approach for the computation of suspended sediment transport. Comparison of measured (dashed line) and computed (solid lines) suspended sediment concentration at the station LT7 (see Figure S2 for the location). The computed suspended sediment concentration was computed by estimating the transport parameter, T, (i) following the probabilistic approach (black bold line, Eq. 3; (ii) using the classic formulation (Eq. 1) without modifying the critical shear stress value (black thin line); (iii) using the classic formulation and reducing the critical shear stress value ($\tau_{cr,S} = 0.3$ Pa; $\tau_{cr,M} = 0.6$ Pa; grey line)

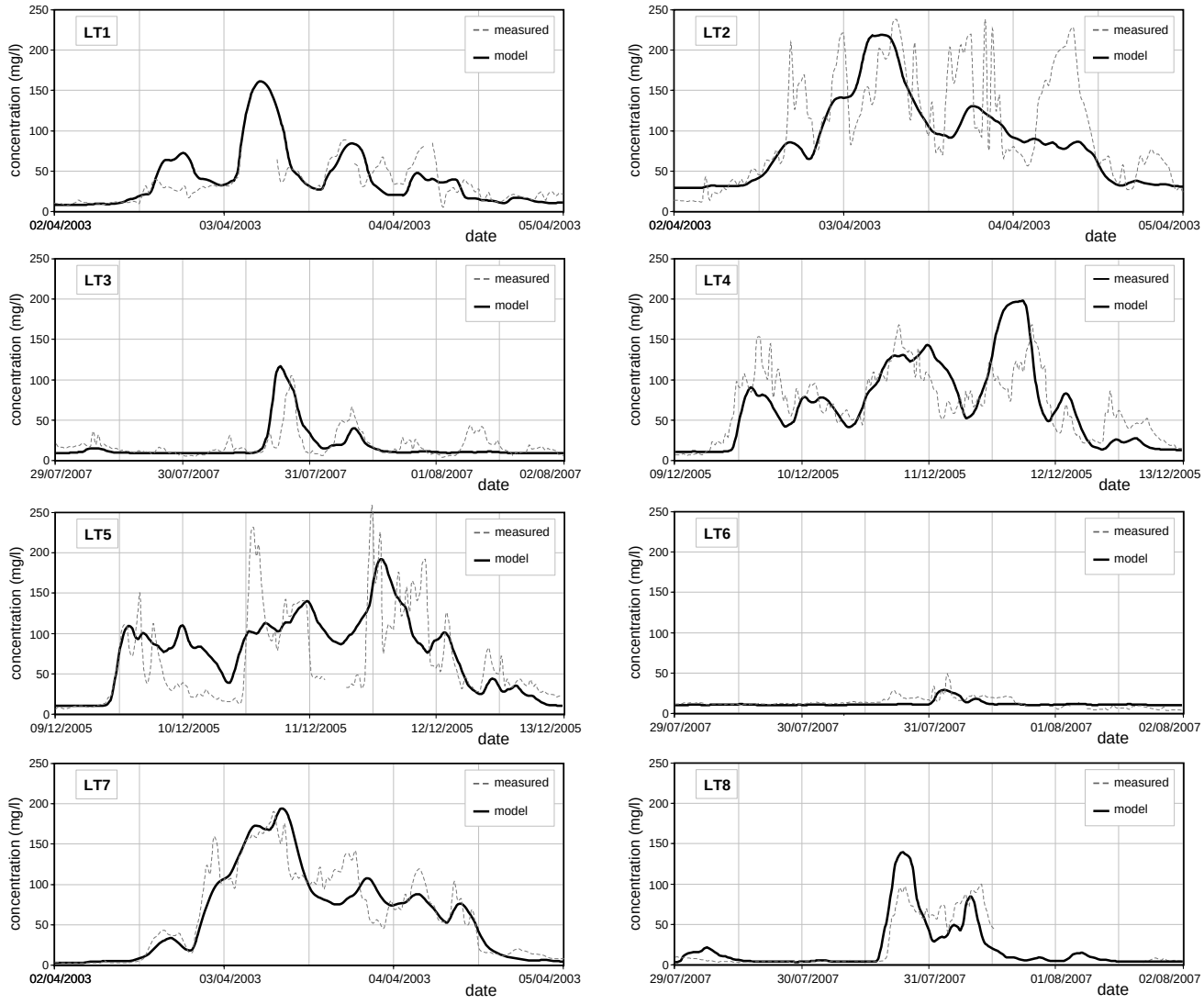

Figure S4. Sediment transport model calibration with intense wind events. Comparison of measured (dashed line) and computed (solid line) suspended sediment concentrations at the stations LT1 to LT8 within the lagoon during intense Bora wind events. See Figure S2 for the position of the stations.

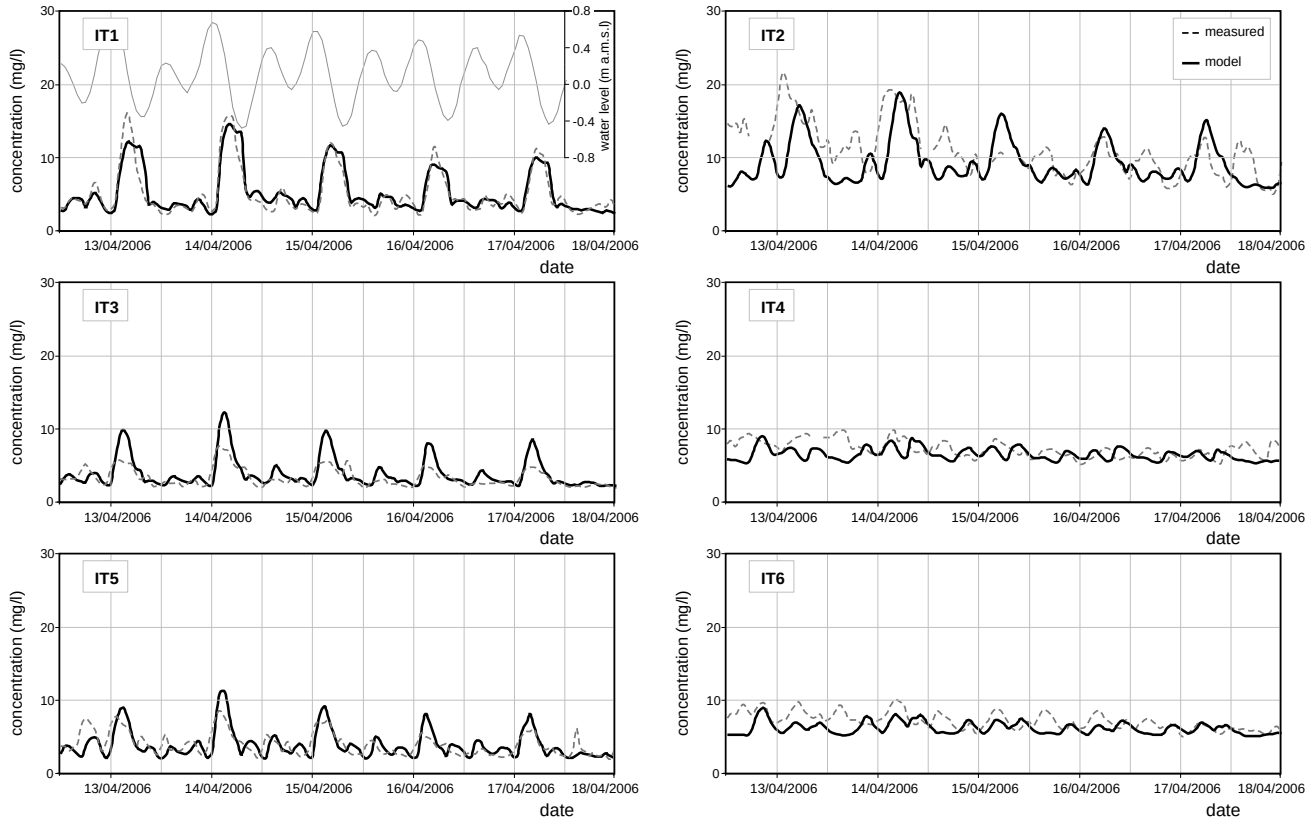

Figure S5. Sediment transport model calibration with weak wind conditions. Comparison of measured (dashed line) and computed (solid line) suspended sediment concentrations at the stations located close to the three inlets (IT) during an event characterized by very low wind conditions. The upper-left plot also shows the water level at the three inlets. See Figure S2 for the position of the stations.

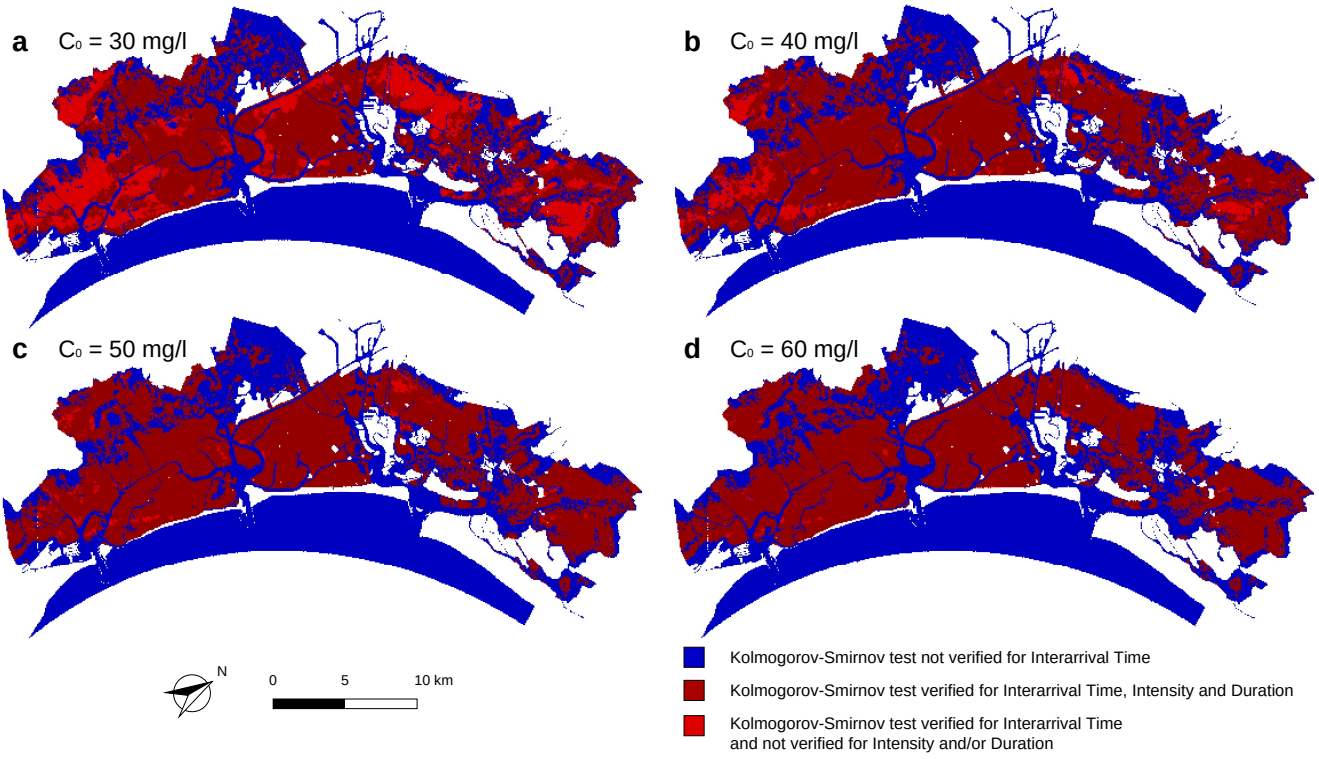

Figure S6. Sensitivity analysis of the threshold C_0. Spatial distribution of Kolmogorov-Smirnov (KS) test at significance level ($\alpha = 0.05$) for different values of the threshold, C_0: (**a**) 30 mg l^{-1}; (**b**) 40 mg l^{-1}; (**c**) 50 mg l^{-1}; (**d**) 60 mg l^{-1}. In the maps we can distinguish areas where the KS test is: not verified (dark blue); verified for all the considered stochastic variables (interarrival time, intensity over the threshold and duration) (dark red); verified for the interarrival time and not for intensity and/or duration (light red). Maps show little to no influence of the threshold value within the selected range on the possibility to model over-threshold SSC events as a Poisson process.

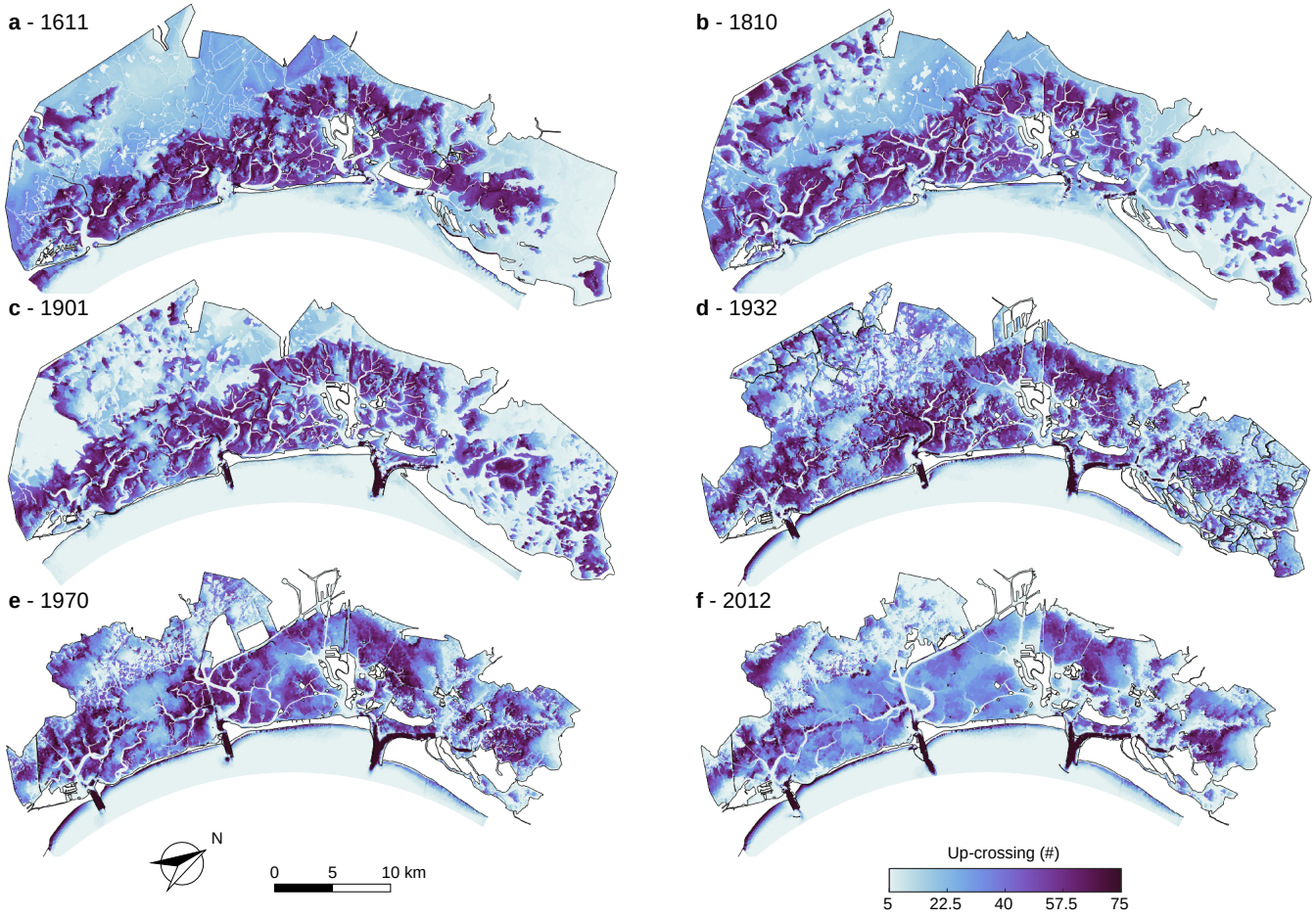

Figure S7. Number of upcrossings of the erosion threshold. Spatial distribution of the number of upcrossings of the threshold for erosion $\tau_c = 0.4$ Pa for the six different configurations of the Venice Lagoon: (**a**) 1611, (**b**) 1810, (**c**) 1901, (**d**) 1932, (**e**) 1970, and (**f**) 2012.

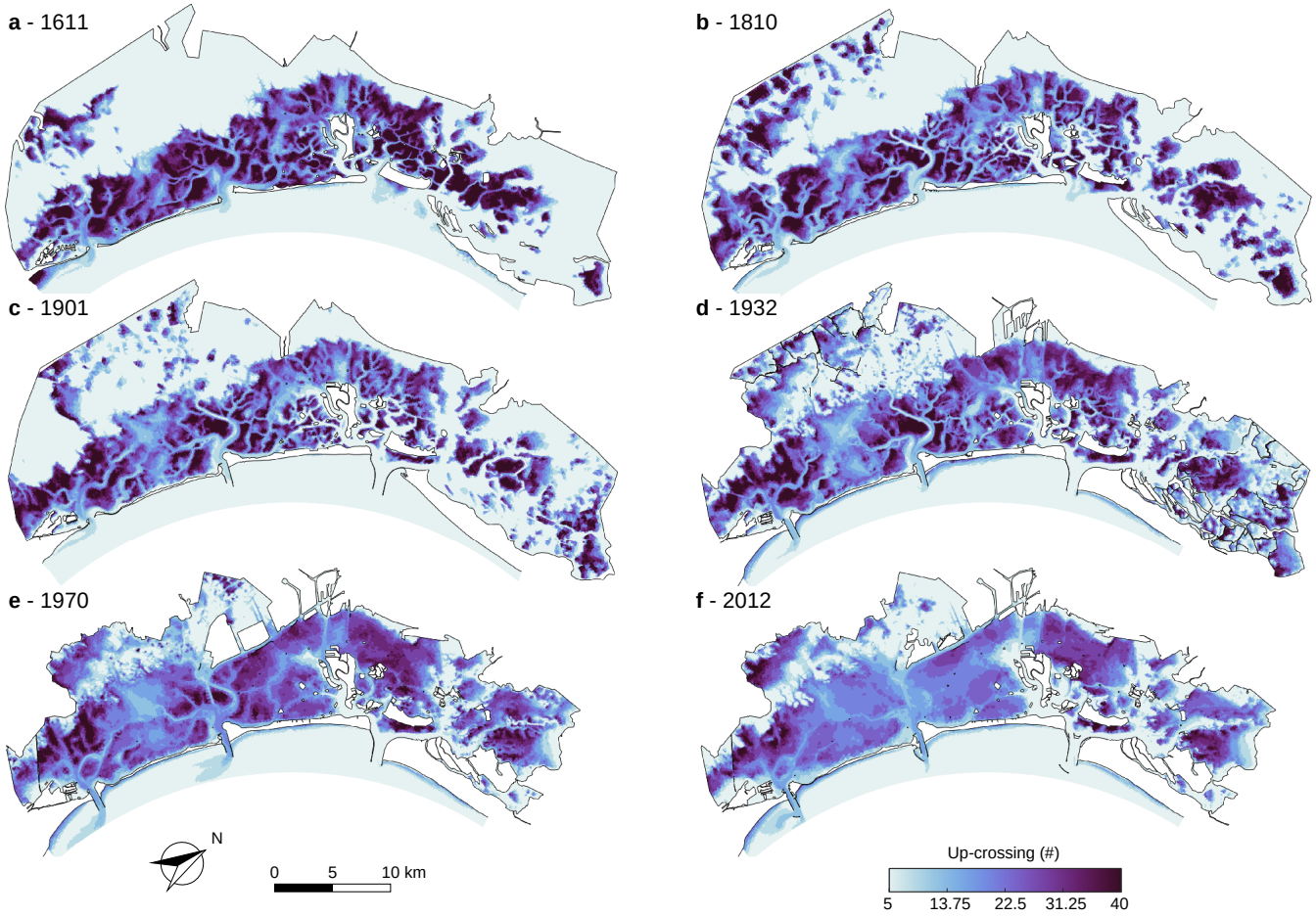

Figure S8. Number of upcrossings of the SSC threshold. Spatial distribution of the number of upcrossing of the threshold for suspended sediment concentration $C_0 = 40$ mg l^{-1}, for the six different configurations of the Venice Lagoon: (**a**) 1611, (**b**) 1810, (**c**) 1901, (**d**) 1932, (**e**) 1970, and (**f**) 2012.

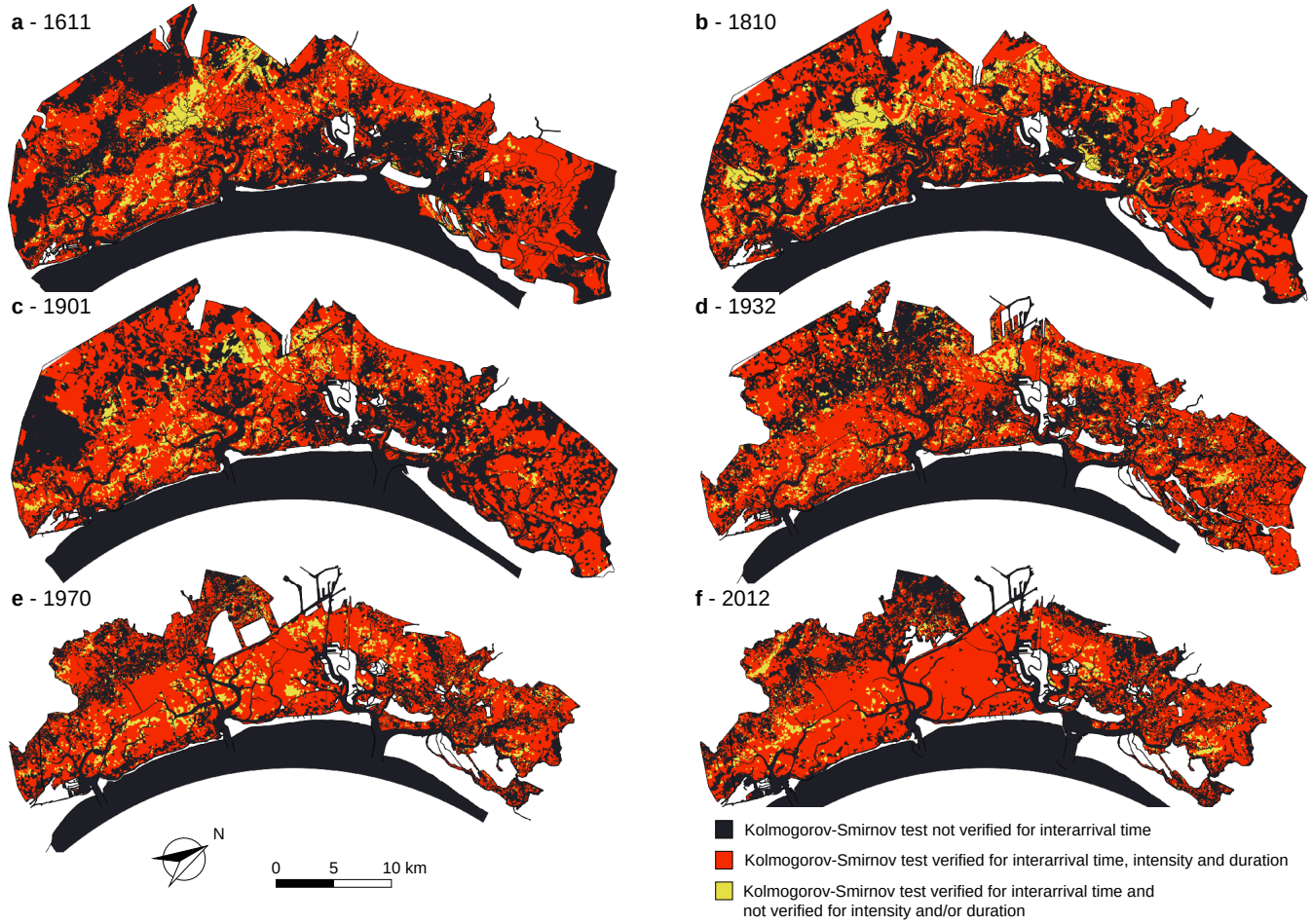

Figure S9. Kolmogorov-Smirnov test for over-threshold erosion events. Spatial distribution of Kolmogorov-Smirnov (KS) test at significance level ($\alpha = 0.05$) for the six different configurations of the Venice Lagoon: (**a**) 1611, (**b**) 1810, (**c**) 1901, (**d**) 1932, (**e**) 1970, and (**f**) 2012. In the maps we can distinguish areas where the KS test is: not verified (dark blue); verified for all the considered stochastic variables (interarrival time, intensity over the threshold and duration) (red); verified for the interarrival time and not for intensity and/or duration (yellow).

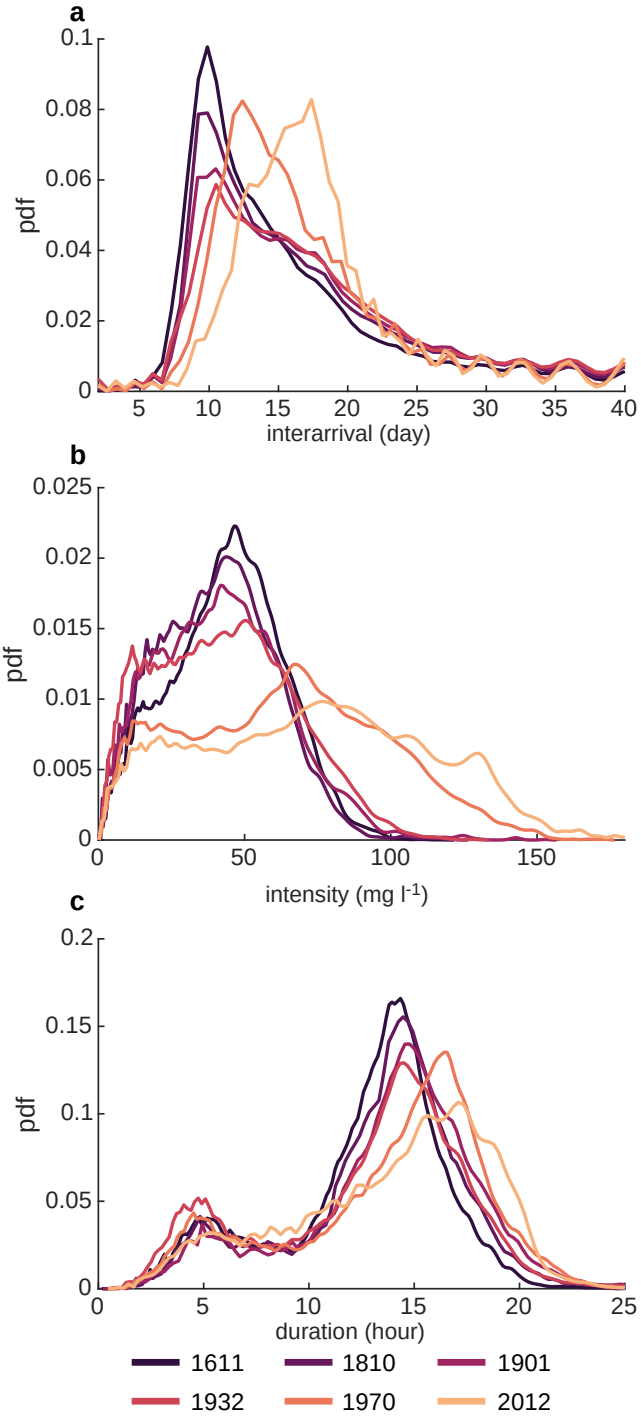

Year	t [day]	
	(mean $\pm$ std)	(median)
1611	27.49 $\pm$ 36.45	14.96
1810	29.35 $\pm$ 36.32	16.47
1901	32.47 $\pm$ 40.30	17.93
1932	33.59 $\pm$ 41.09	18.31
1970	27.87 $\pm$ 32.87	16.47
2012	29.24 $\pm$ 32.25	17.95

Year	e [mg l^{-1}]	
	(mean $\pm$ std)	(median)
1611	44.20 $\pm$ 19.00	44.99
1810	40.84 $\pm$ 19.17	41.05
1901	42.66 $\pm$ 21.80	41.96
1932	43.49 $\pm$ 23.36	42.95
1970	64.16 $\pm$ 33.86	65.02
2012	73.21 $\pm$ 38.85	74.68

Year	d [hour]	
	(mean $\pm$ std)	(median)
1611	12.58 $\pm$ 3.91	13.50
1810	13.23 $\pm$ 4.12	14.02
1901	13.78 $\pm$ 4.27	14.46
1932	12.71 $\pm$ 4.71	13.85
1970	13.76 $\pm$ 4.73	14.98
2012	13.96 $\pm$ 4.70	14.96

Figure S10. Spatial probability density function of interarrival time, intensity and duration of SSC over-threshold events. Probability density function (left), mean (mean $\pm$ standard deviation) and median value (right) of interarrival times t (**a**), intensity e (**b**) and duration d (**c**) of SSC over-threshold events.

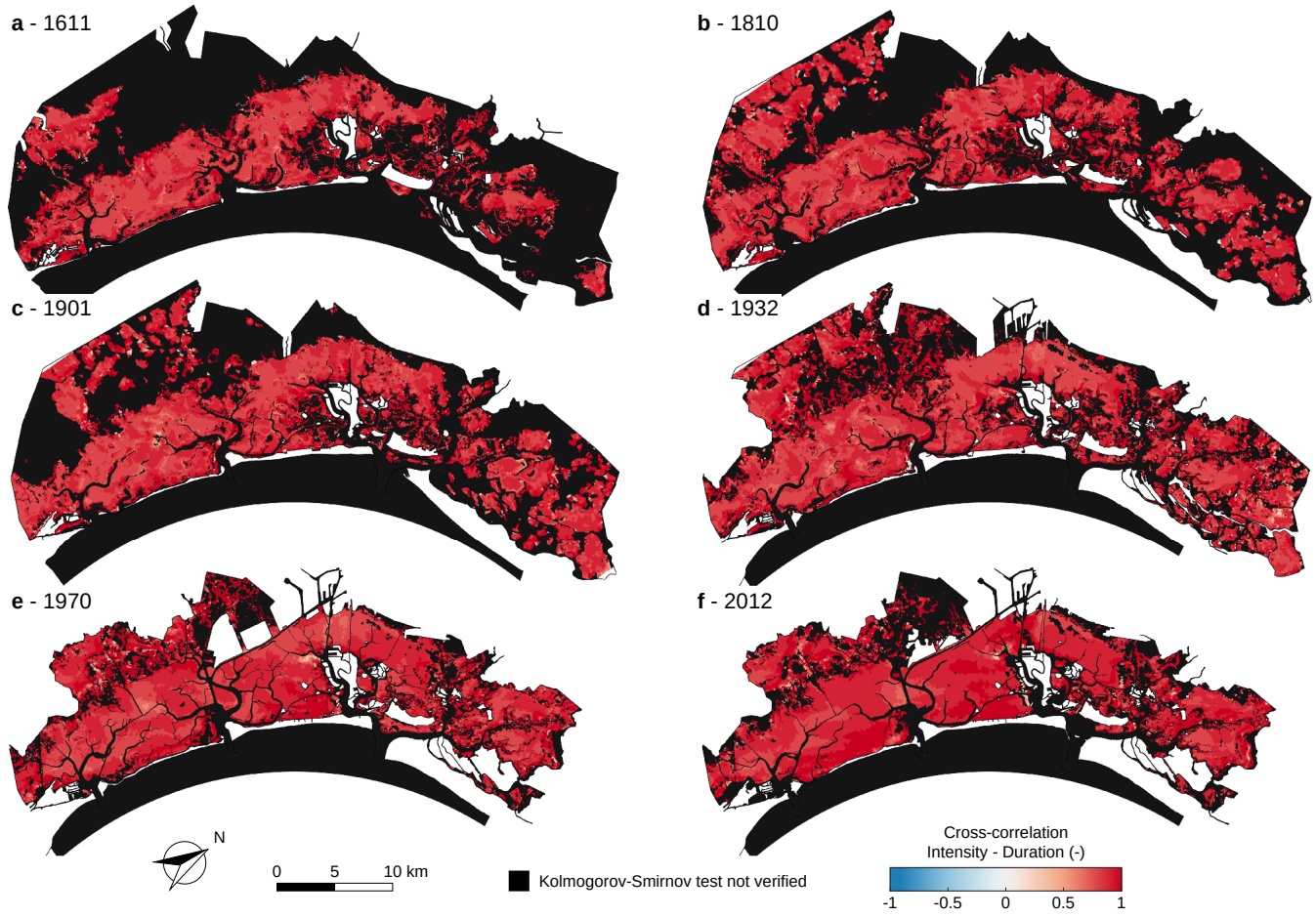

Figure S11. Cross-correlation between intensity and duration over-threshold SSC events. Spatial distribution of temporal cross-correlation between intensity of peak-excesses and duration of over-threshold exceedances for the six different configurations of the Venice Lagoon: (**a**) 1611, (**b**) 1810, (**c**) 1901, (**d**) 1932, (**e**) 1970, and (**f**) 2012. Black identifies sites where over-threshold SSC events cannot be modeled as a marked Poisson process (i.e. the KS test is not verified for the interarrival time).

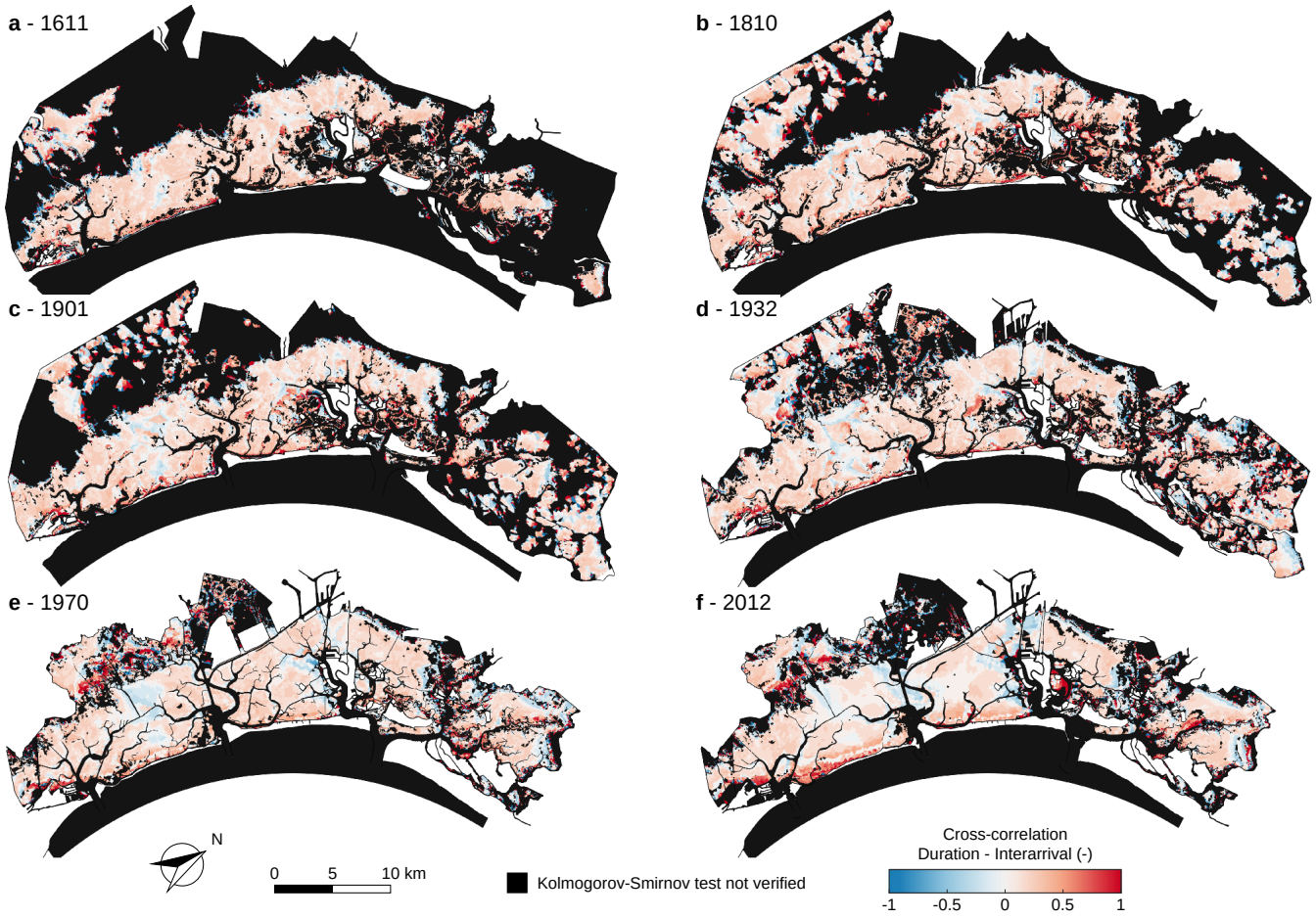

Figure S12. Cross-correlation between duration and interarrival times over-threshold SSC events. Spatial distribution of temporal cross-correlation between duration and interarrival times of over-threshold exceedances for the six different configurations of the Venice Lagoon: (**a**) 1611, (**b**) 1810, (**c**) 1901, (**d**) 1932, (**e**) 1970, and (**f**) 2012. Black identifies sites where over-threshold SSC events cannot be modeled as a marked Poisson process (i.e. the KS test is not verified for the interarrival time).

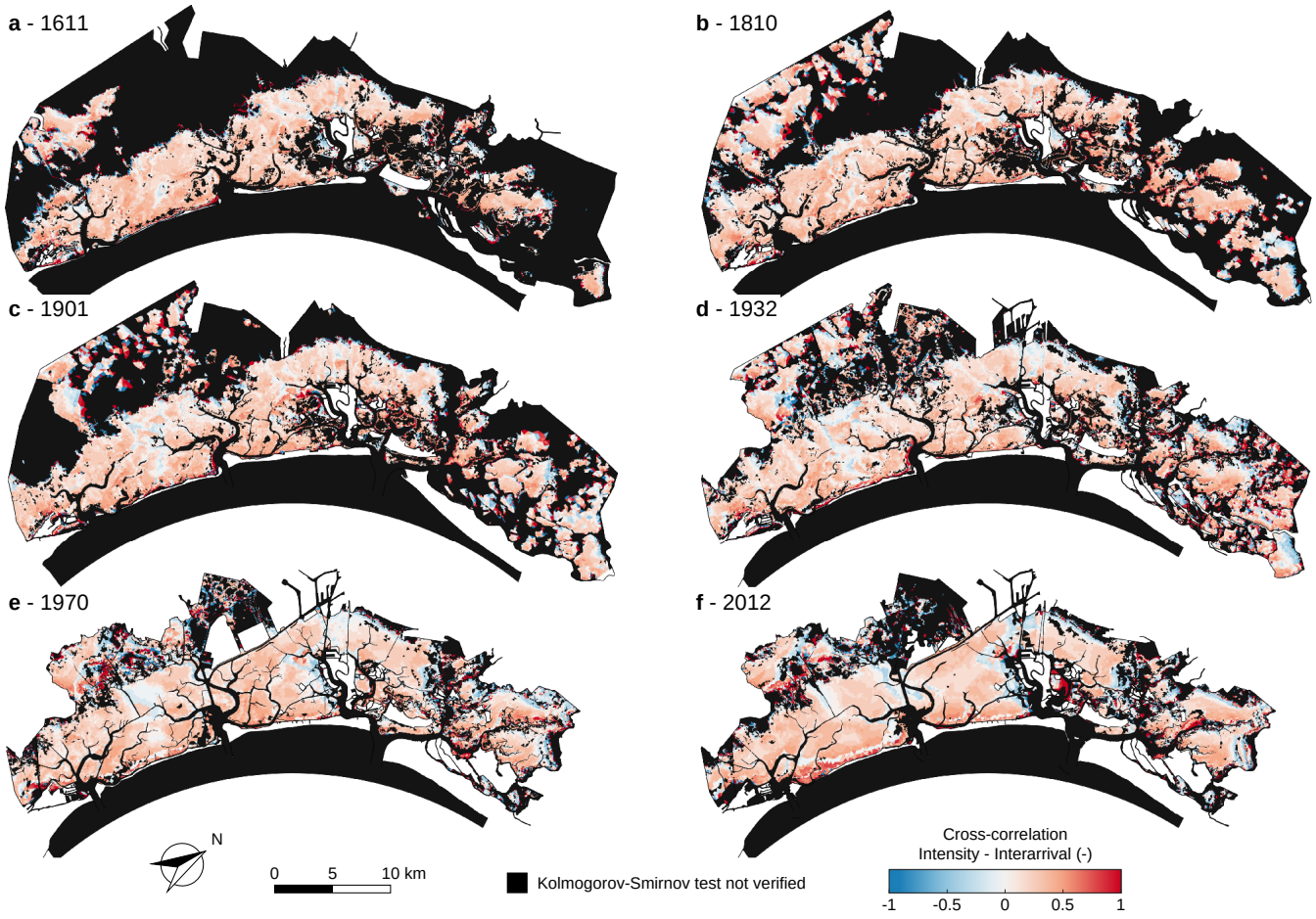

Figure S13. Cross-correlation between intensity and interarrival times of over-threshold SSC events. Spatial distribution of temporal cross-correlation between intensity of peak-excesses and interarrival times of over-threshold exceedances for the six different configurations of the Venice Lagoon: (**a**) 1611, (**b**) 1810, (**c**) 1901, (**d**) 1932, (**e**) 1970, and (**f**) 2012. Black identifies sites where over-threshold SSC events cannot be modeled as a marked Poisson process (i.e. the KS test is not verified for the interarrival time).

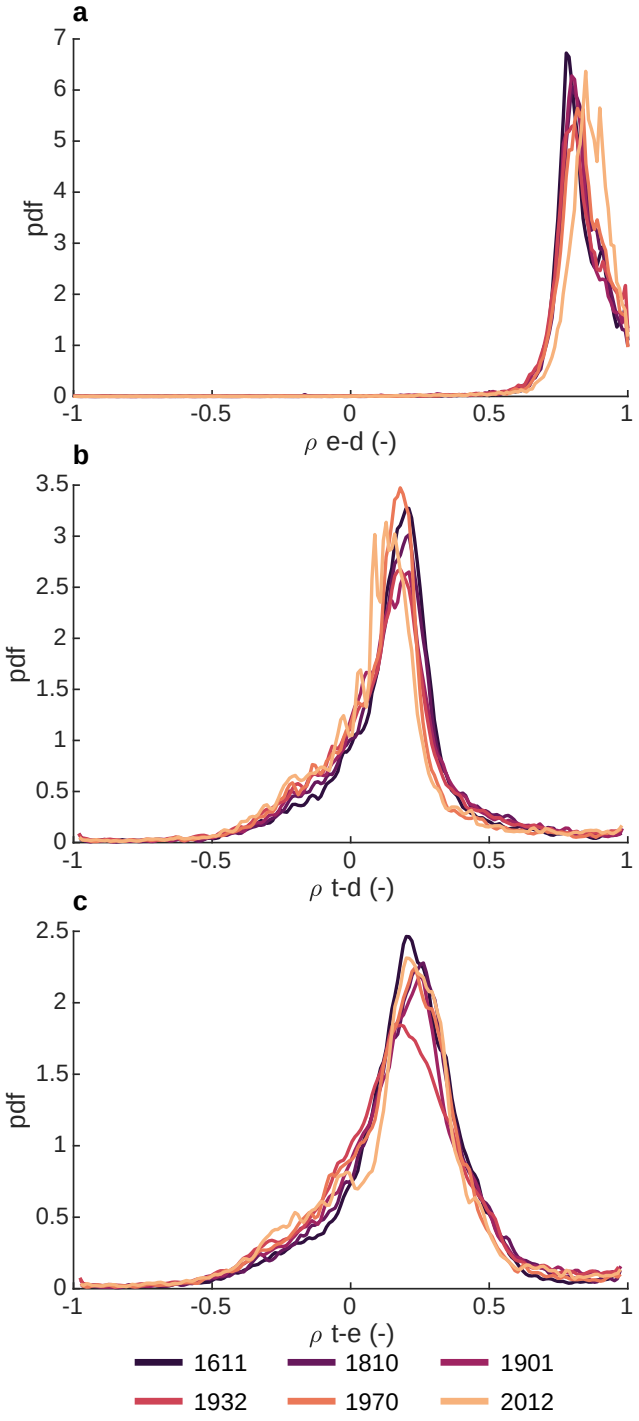

Year	$\rho(e-d)$ [-] (mean $\pm$ std)
1611	0.81 ± 0.10
1810	0.82 ± 0.11
1901	0.81 ± 0.11
1932	0.81 ± 0.12
1970	0.83 ± 0.10
2012	0.85 ± 0.10

Year	$\rho(t-d)$ [-] (mean $\pm$ std)
1611	0.14 ± 0.30
1810	0.15 ± 0.30
1901	0.13 ± 0.32
1932	0.12 ± 0.33
1970	0.11 ± 0.29
2012	0.10 ± 0.31

Year	$\rho(t-e)$ [-] (mean $\pm$ std)
1611	0.18 ± 0.30
1810	0.19 ± 0.31
1901	0.18 ± 0.33
1932	0.16 ± 0.34
1970	0.16 ± 0.30
2012	0.16 ± 0.32

Figure S14. Spatial probability density function of cross-correlation between interarrival time, intensity and duration of SSC over-threshold events. Probability density function (left) and mean value (mean $\pm$ standard deviation, right) of cross-correlation between intesity and duration $\rho(e-d)$ (**a**), interarrival time and duration $\rho(t-d)$ (**b**) and interarrival time and intensity $\rho(t-e)$ (**c**).

References

Allen, J. I., Somerfield, P. J., and Gilbert, F. J.: Quantifying uncertainty in high-resolution coupled hydrodynamic-ecosystem models, Journal of Marine Systems, 64, 3–14, https://doi.org/10.1016/j.jmarsys.2006.02.010, 2007.

Bridge, J. S. and Bennett, S. J.: A model for the entrainment and transport of sediment grains of mixed sizes, shapes, and densities, Water Resources Research, 28, 337–363, https://doi.org/https://doi.org/10.1029/91WR02570, 1992.

Carniello, L., Defina, A., and D'Alpaos, L.: Modeling sand-mud transport induced by tidal currents and wind waves in shallow microtidal basins: Application to the Venice Lagoon (Italy), Estuarine, Coastal and Shelf Science, 102-103, 105–115, https://doi.org/10.1016/j.ecss.2012.03.016, 2012.

Grass, A. J.: Initial Instability of Fine Bed Sand, Journal of the Hydraulics Division, 96, 619–632, https://doi.org/10.1061/JYCEAJ.0002369, 1970.